Uniform and Non-Uniform Pumping Effect on Ce:Nd:YAG Side-Pumped Solar Laser Output Performance

Cláudia R. Vistas [1], Dawei Liang [1,*], Dário Garcia [1], Miguel Catela [1], Bruno D. Tibúrcio [1], Hugo Costa [1], Emmanuel Guillot [2] and Joana Almeida [1]

[1] Centro de Física e Investigação Tecnológica, Departamento de Física, Faculdade de Ciências e Tecnologia, Universidade NOVA de Lisboa, 2829-516 Caparica, Portugal; c.vistas@fct.unl.pt (C.R.V.); kongming.dario@gmail.com (D.G.); m.catela@campus.fct.unl.pt (M.C.); brunotiburcio78@gmail.com (B.D.T.); hf.costa@campus.fct.unl.pt (H.C.); jla@fct.unl.pt (J.A.)
[2] PROMES-CNRS, 7 rue du Four Solaire, 66120 Font Romeu, France; emmanuel.guillot@promes.cnrs.fr
*   Correspondence: dl@fct.unl.pt

Abstract: The Ce:Nd:YAG is a recent active medium in solar-pumped lasers with great potential. This study focuses on the influence of two secondary concentrators: a fused silica aspherical lens and a rectangular fused silica light guide; and consequent pump light distribution on the output performance of a Ce:Nd:YAG side-pumped solar laser. The solar laser head with the aspherical lens concentrated the incident pump light on the central region of the rod, producing the highest continuous-wave 1064 nm solar laser power of 19.6 W from the Ce:Nd:YAG medium. However, the non-uniformity of the absorbed pump profile produced by the aspherical lens led to the rod fracture because of the high thermal load, limiting the maximum laser power. Nevertheless, the solar laser head with the light guide uniformly spread the pump light along the laser rod, minimizing the thermal load issues and producing a maximum laser power of 17.4 W. Despite the slight decrease in laser power, the use of the light guide avoided the laser rod fracture, demonstrating its potential to scale to higher laser power. Therefore, the pumping distribution on the rod may play a fundamental role for Ce:Nd:YAG solar laser systems design.

Keywords: Ce:Nd:YAG; aspherical lens; light guide; solar laser; side-pumped; uniformity

1. Introduction

The direct conversion of sunlight into laser radiation by solar-pumped lasers is of interest for several laser-based applications such as free-space optical communications, laser propulsion, space-to-Earth wireless power transmission, asteroid deflection, and photovoltaic energy conversion [1–3]. Since early research of solar-pumped laser in the 1960s [4,5], the research of Arashi et al. in 1984 [6], Weskler et al. in 1988 [7], Lando et al. in 2003 [8], Dinh et al. in 2012 [9] and Liang et al. in 2018 [10] have revealed considerable progresses on optical pumping approaches in order to obtain a better solar laser output efficiency. The optical pumping design relies on primary, secondary and tertiary concentrators to achieve enough pumping intensity for the lasing threshold. Primary concentrators, namely parabolic mirrors and Fresnel lenses, collect and concentrate the solar radiation to a focal zone, where a solar laser head is introduced. Secondary concentrators, such as aspheric lenses and light guides, concentrate and distribute the solar light rays from the focal zone of the primary concentrator to the laser-active medium. Tertiary concentrators, such as 2D compound parabolic concentrators (CPCs), 3D CPCs, and V-shaped pump cavities, are also indispensable for high-flux pumping of the laser medium since they can either compress or wrap the concentrated solar radiation from their input aperture to the laser-active medium. Two most widely used methods of solar pumping are end-side-pumping [9–17] and side-pumping [8,18–23]. Although the end-side-pumping approach allows greater laser efficiency, the distribution of pump light is non-uniform, which may lead to serious

thermal loading problems [12]. This issue is countered by using the side-pumping method as it allows a more uniform light distribution along the rod axis, spreading the absorbed power within the medium.

The most popular laser gain medium is the Nd:YAG because of its excellent spectroscopic, mechanical, and thermal properties. However, the prominent drawback of the Nd:YAG medium is the poor overlap of its narrow absorption bands with the solar spectrum.

Sensitizers of the Nd^{3+} ion emission, such as Ce^{3+} and Cr^{3+} ions, can be added as co-dopants in the doped YAG host to increase the efficiency of solid-state lasers by absorbing more light from broadband radiation, transferring the excitation energy to the Nd^{3+} ions (discussed below).

The Cr:Nd:YAG active medium has been used in solar-pumped lasers; however, the gain has not been significantly greater than what would be theoretically expected [10,14,24]. The record collection efficiency is 32.5 W/m^2 for an end-side-pumped solar laser using a Cr:Nd:YAG ceramic rod [10]. Nevertheless, this value is only 1.03 and 1.01 times higher than that of a Nd:YAG single-crystal rod [14] and a bonding Nd:YAG/YAG crystal rod [16], respectively.

Just recently, the Ce:Nd:YAG medium was tested in solar lasers by using end-side-pumping [25] and side-pumping [26] configurations. The former produced a lower output power compared with that of the Nd:YAG solar laser under the same solar pump power [25]. This can result from the larger scattering loss within the crystal attributed to the Ce co-dopant, but also from the thermal load on the Ce:Nd:YAG rod by using an end-side-pumping configuration, causing the final fracture of the rod [25]. Therefore, in the most recent study, a side-pumping configuration was used to allow a uniform pump light absorption and homogeneous laser rod heating [26]. This led to a significant increase in the solar laser efficiency, obtaining the record 23.6 W/m^2 collection efficiency for a side-pumping configuration, which was 1.57 times higher than the one obtained with a Nd:YAG solar laser under the same pumping conditions [26].

It is interesting to note that the thermal loading issues are not manifested in the same manner in the Nd:YAG and Ce:Nd:YAG active media. The fracture of a Nd:YAG laser rod already occurred in an end-side-pumped solar laser configuration. However, its incoming solar power was at a much higher level of 2585 W [12] compared with the only 964 W incoming power for the Ce:Nd:YAG rod also in an end-side-pumped solar laser configuration [25]. The main reason behind this difference may rely on the Stokes shift. The Stokes shift (η_s) is the spectral difference between the emission ($\lambda_{Emission}$) and the pump (λ_{Pump}) peak wavelengths. The Nd:YAG pumped by sunlight has a Stokes efficiency of 0.62 ($\eta_s = \lambda_{Pump}/\lambda_{Emission} = 660$ nm/1064 nm = 0.62 [7]); thereby, 38% of the pump photon energy is dissipated as heat to the crystal. The Ce:Nd:YAG has a lower Stokes efficiency of about 0.43 ($\eta_s = \lambda_{Pump}/\lambda_{Laser} = 460$ nm/1064 nm = 0.43 [27]); thus, about 57% of the energy of every pump photon transferred from Ce^{3+} to Nd^{3+} ions is lost. This lower Stokes efficiency results in a higher thermal load on the active medium. Therefore, the thermal effects were more pronounced under solar pumping, leading the Ce:Nd:YAG rod to fracture more easily [25] compared with the Nd:YAG rod [12,14].

Since the thermal loading issues play a vital role in the design of Ce:Nd:YAG solar laser systems, it is important to consider the solar pumping distribution along the laser rod on the optimization process of solar laser power scaling. Although the side-pumping configuration may allow a more uniform light distribution along the rod compared with the end-side-pumping configuration it is the secondary concentrator that plays a fundamental role in the distribution and uniformization of the light rays. The two most used secondary concentrators in side-pumped solar lasers are the fused silica aspherical lens [13,14,18,23] and fused silica light guide [19,21,22]. Even though these concentrators have been frequently applied in solar laser prototypes, a comparative study between them to evaluate their performance on solar lasers is still lacking. Since Ce:Nd:YAG is a new and potential active medium in solar-pumped lasers, it is important to study the effect of the pump light distribution on its performance. Therefore, this study is focused on the influence

of these secondary concentrators and consequent pump light distribution on the output performance of the Ce:Nd:YAG side-pumped solar laser.

2. Optical Spectra and Energy Transfer from Ce^{3+} to Nd^{3+} Ions in Ce:Nd:YAG Medium

The Ce:Nd:YAG active medium has already demonstrated the potential to increase the efficiency of broadband-pumped lasers, compared with the Nd:YAG crystal [28–32] because of its strong absorption in ultraviolet (UV) and visible spectral regions at broadband light pumping and efficient energy transfer from Ce^{3+} to Nd^{3+}. The solar irradiance spectrum, the Nd:YAG and Ce:Nd:YAG absorption spectra, and the Ce:YAG fluorescence spectrum are represented in Figure 1. The Ce:Nd:YAG absorption spectrum has two broad absorption bands centered at 339 nm and 460 nm, which are characteristic of the Ce^{3+} ion in YAG lattice and other bands that are characteristic of the Nd^{3+} ions. The Ce:YAG fluorescence spectrum has a strong and broad green luminescence centered around 531 nm that overlaps well with two absorption peaks of the Nd^{3+} ion around 530 nm and 589 nm.
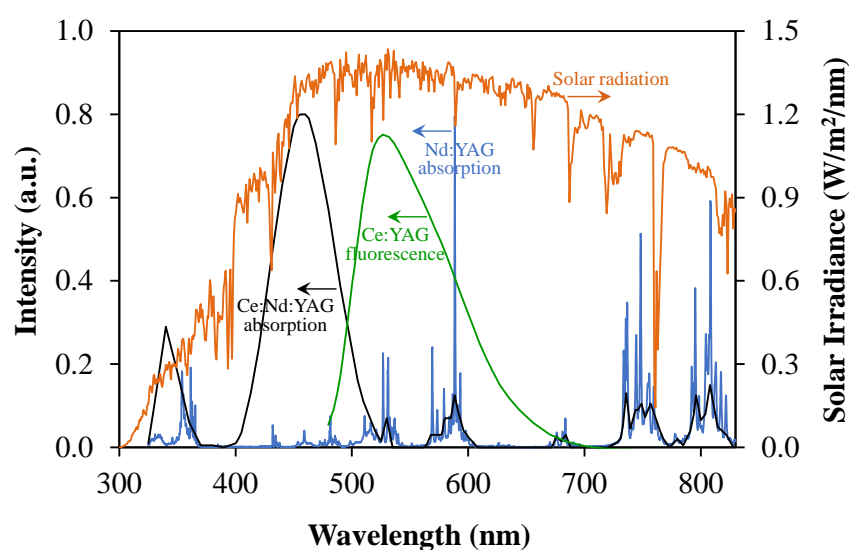
Figure 1. Standard solar emission spectrum (orange line) [33], Ce:YAG fluorescence spectrum (green line) (adapted from [34]), Nd:YAG (blue line) (adapted from [35]), and Ce:Nd:YAG (black line) (adapted from [36]) absorption spectra.

The energy transfer mechanisms in Ce:Nd:YAG material have been investigated in several studies [28–30,36–38]. Radiative energy transfer between Ce^{3+} and Nd^{3+} ions has been previously proved by the superposition of the emission and absorption bands between the two ions [28–30,36–38]. Tai et al. demonstrated another possibility of energy transfer mechanism by near-infrared (NIR) quantum cutting involving the down-conversion of an absorbed visible photon to the emission of two NIR photons [36]. In Figure 2 the energy transfer mechanisms between Ce^{3+} and Nd^{3+} ions are depicted in an energy level diagram. When pump photons at wavelengths around 339 nm and 460 nm are absorbed, the Ce^{3+} ions are excited from the $^2F_{5/2}$ ground state to the broad pump bands 5d$_2$ and 5d$_1$, respectively. The electrons in the 5d$_2$ ($^2B_{1g}$) pump band can relax non-radiatively to the lower 5d$_1$ ($^2A_{1g}$) pump band and then decay radiatively to the $^2F_{5/2}$ ground state. The radiative transfer mechanism occurs between the transition 5d$_1$ ($^2A_{1g}$) $\rightarrow$ $^2F_{5/2}$ of Ce^{3+} ion and the transition $^4I_{9/2}$ $\rightarrow$ $^2G_{7/2}$ of Nd^{3+} ion, because of the strong overlap between the Ce^{3+} emission band and the Nd^{3+} absorption line, as shown in Figures 1 and 2, indicated by pathway (1) [28–30,36–38] through the cross-relaxation process. The other energy transfer mechanism based on the cooperative down-conversion is possible because the energy of the transition 5d$_1$ ($^2A_{1g}$) $\rightarrow$ $^2F_{5/2}$ of Ce^{3+} ion is approximately twice as high as the energy difference between the $^4F_{3/2}$ and $^4I_{11/2}$ levels of the Nd^{3+} ion (Figure 2, as shown by pathway (2)) [36,39,40].
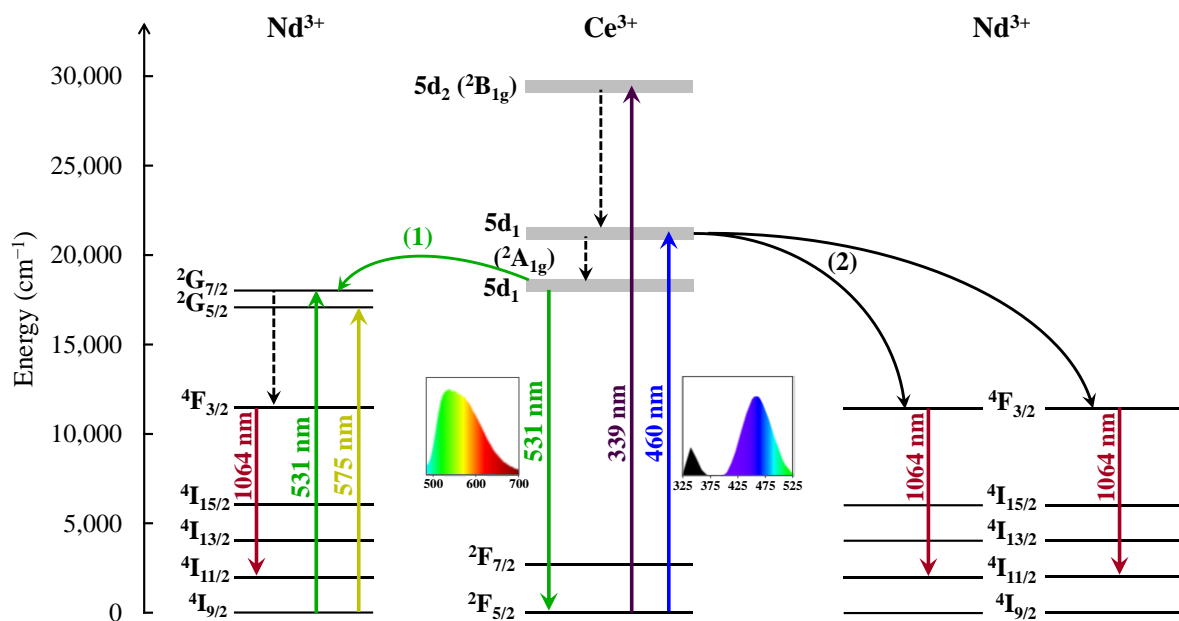
Figure 2. Energy-level diagram illustrating the energy transfer mechanisms between Ce^{3+} and Nd^{3+} ions in the Ce:Nd:YAG active medium (adapted from [36]). (1) Radiative energy transfer pathway. (2) Quantum cutting down-conversion pathway.

The good overlap between the Ce^{3+} absorption bands and the solar spectrum (Figure 1) in addition to the efficient energy transfer between Ce^{3+} and Nd^{3+} ions (Figure 2) make the Ce:Nd:YAG active medium of particular interest to solar-pumped laser researchers.

3. Solar-Pumped Ce:Nd:YAG Laser Systems

3.1. PROMES-CNRS Heliostat-Parabolic Mirror Solar Energy Collection and Concentration System

The medium size solar furnace (MSSF) of Procédés, Matériaux et Énergie Solaire—Centre National de la Recherche Scientifique (PROMES-CNRS) was used for the solar laser experiments. The incoming solar radiation was redirected by a large plane mirror (3.0 m × 3.0 m) with 36 small flat segments (0.5 m × 0.5 m each) mounted on a two-axis heliostat towards the stationary parabolic mirror with 2 m diameter, 60° rim angle, and 850 mm focal length (Figure 3). The external annular area of the parabolic mirror was masked to avoid overheating the gain medium so that only 1.38 m in diameter of its central circular area was used. An effective solar collection area of 1.09 m^2 was calculated after discounting the shading effects of a shutter, X-Y-Z axis positioner, solar laser cavity and 0.3 m diameter central opening of the parabolic mirror. The shutter was used to control the input power. All the mirrors of the MSSF solar facility are back-surface silver-coated, and because of the iron impurities within the glass substrates and imperfections, only 59% of incoming solar radiation was focused to the focal zone. Direct solar irradiances between 1036 W/m^2 and 1061 W/m^2 were measured during the experiments in Odeillo (France), in February 2022. A Kipp and Zonen CH1 pyrheliometer, on a Kipp and Zonen 2AP solar tracker, from Kipp and Zonen, Delft, The Netherlands, was used for the measurements.
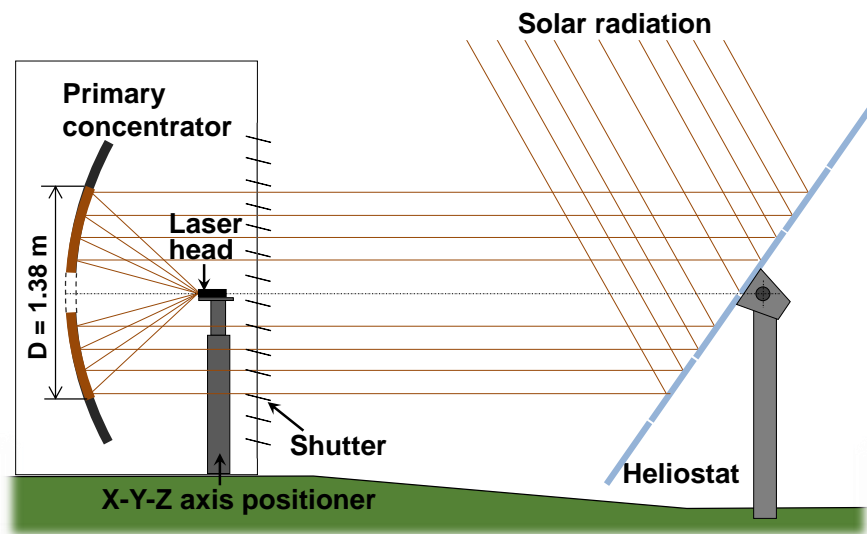
Figure 3. Schematics of the PROMES-CNRS solar energy collection and concentration system.

3.2. Side-Pumped Ce:Nd:YAG Solar Laser Heads

Two solar laser heads were investigated using as secondary concentrator: (1) a fused silica aspherical lens, and (2) a fused silica light guide with rectangular cross-section, as shown in Figures 4 and 5.
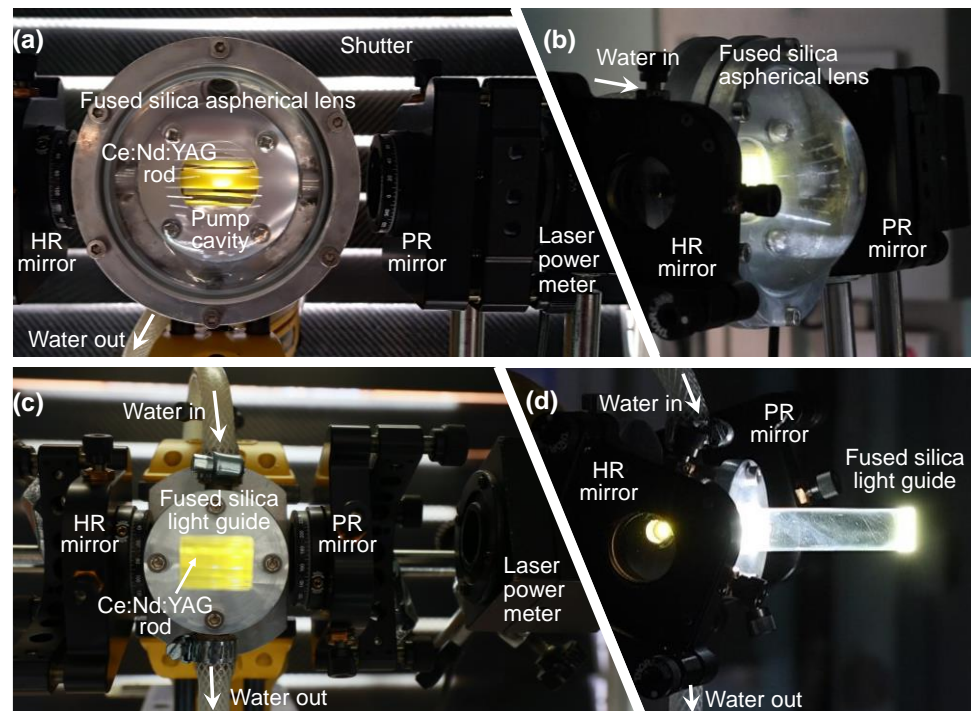
Figure 4. Photographs of the front view (**a**,**c**) and side view (**b**,**d**) of the Ce:Nd:YAG solar laser heads using the fused silica aspherical lens (**a**,**b**) and the fused silica light guide (**c**,**d**). PR: partial reflection; HR: high reflection.
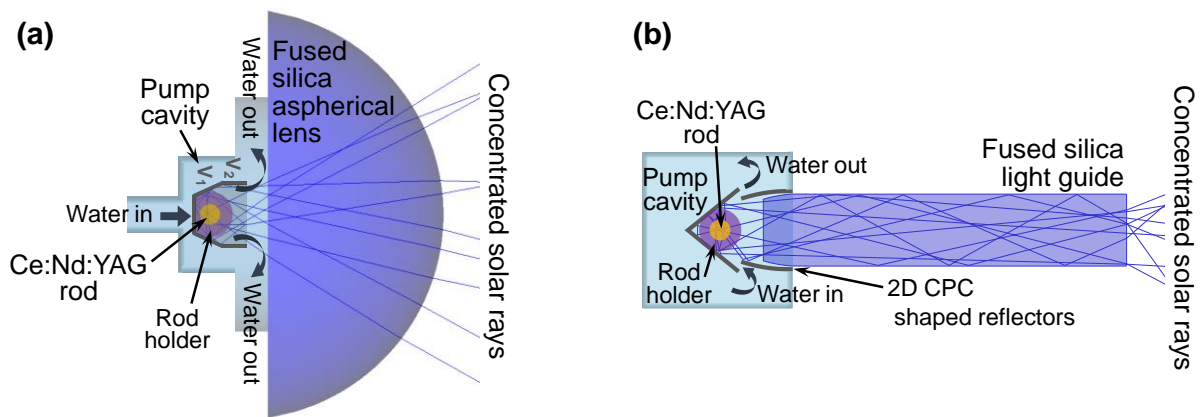
Figure 5. Schematics of the side-view of the solar laser heads with aspherical lens (**a**) and with light guide (**b**).

The aspherical lens of the first laser head was fabricated of fused silica material, which has a low coefficient of thermal expansion, being resistant to thermal shock, and a wide transparency range, which can extend from the UV into the NIR. It had 80 mm diameter, 60 mm radius of curvature, and 35 mm thickness. This laser head had also a tertiary concentrator constituted by a 2D pumping cavity, which had a trapezoidal-shaped reflector V_1 with a 25° opening angle, and two upper planar reflectors V_2 perpendicular to the bottom face of the pumping cavity (Figure 5a), enabling an effective coupling of the concentrated light rays with different incident angles into the rod [26]. This pumping cavity, covered with a 94%-reflectivity silver-coated aluminum foil, had an entrance aperture of 12.2 mm × 22.0 mm, a depth of 13.3 mm and an 11.0 mm separation between the plane output face of the aspherical lens and the laser rod optical axis.

The second laser head used a rectangular light guide also fabricated of fused silica material with 73.5 mm length, 14 mm × 18.4 mm input end, and an output section with the shape of a 2D CPC with 5.5 mm length and 12 mm × 22 mm output end. As tertiary concentrator, this laser head had a 2D V-shaped pump cavity with 16 mm × 22 mm entrance aperture and 10 mm depth, positioned at the exit of 2D CPC shaped reflectors with 12 mm × 22 mm output end (Figure 5b). All these provided an efficient coupling of the light to the laser rod. The inner walls of both the V-shaped and upper part of the pump cavity were bonded with a protected silver-coated aluminum foil with 94% reflectivity.

The active medium investigated was a Ce(0.1%):Nd(1.1%):YAG rod of 4.0 mm diameter and 35 mm length with both end faces polished and anti-reflection coated for the laser emission wavelength (reflectivity (R) < 0.2% @ 1064 nm), supplied by Chengdu Dongjun Laser Co., Ltd. (Chengdu, China). This rod had a refractive index = 1.8197 @ 1064 nm; perpendicularity < 3′, parallelism < 10″, flatness < 1/10λ; surface quality = 20/10; and damage threshold ≥ 5 J/cm^2 @ 1064 nm, 10 ns 10 Hz. The laser rod was mounted inside the pump cavity of each laser head. Both the cavity and the laser rod were actively cooled by water with 6 L/min flow rate.

Each solar laser head was fixed on the X-Y-Z axis positioner, ensuring a precise optical alignment in the focal zone. A high reflection (HR) coated flat mirror at 1064 nm (99.96% @ 1064 nm) and a partial reflection (PR) coated flat output coupler at 1064 nm (R ≥ 95% @ 1064 nm) constituted the optical resonator of short length. The laser output power was measured with a Thorlabs PM1100D power meter.

The laser beam quality M^2 factors were determined by measuring the beam diameter at $1/e^2$ at a near-field position (75 mm from the output coupler) and a far-field position (1.0 m away from the output coupler). The laser beam divergence θ was found using Equation (1):

$$\tan \theta = (\phi_2 - \phi_1) / 2L \tag{1}$$

where ϕ_1 and ϕ_2 are the measured laser beam diameters at $1/e^2$ width, 75 mm, and 1.0 m away from the output mirror, respectively, and L is the distance between these two points. The M^2 factor was then calculated by Equation (2):

$$M^2 = \theta/\theta_0 \qquad (2)$$

where $\theta_0 = \lambda/\pi\omega_0$ is the divergence of diffraction-limited Gaussian beam for λ = 1.064 μm and ω_0 is the beam waist radius, as calculated by LASCAD analysis for the 4 mm diameter rod within the symmetric laser resonator. This value can be confirmed by measuring the laser beam diameter at $1/e^2$ width ϕ_1 at near-field position.

4. Ce:Nd:YAG Side-Pumped Solar Laser Experiments with Either the Aspherical Lens or the Light Guide

Two side-pumped solar laser heads were investigated to study the influence of the secondary concentrators, aspherical lens and rectangular light guide, on the Ce:Nd:YAG output performance.

Aspherical lenses have a non-spherical surface, in which the radius of curvature gradually changes from the center of the lens to the edge, having a shape slightly divergent from spherical. The function of this asphere surface is to reduce or eliminate spherical aberration, an optical effect that causes incident light rays to focus on different points. Therefore, aspherical lenses can focus all the incident light on the exact same point, providing true diffraction-limited spot sizes and the lowest wavefront error. With aspherical lenses, the concentrated solar radiation can be collected and compressed efficiently from the focal zone of the parabolic mirror into the laser rod.
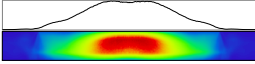
Rectangular light guides transmit the incident light through internal refractive and total internal reflection principles to a particular area. In solar-pumped lasers, they are used to distribute and uniform the concentrated solar radiation from the focal zone along the laser rod.
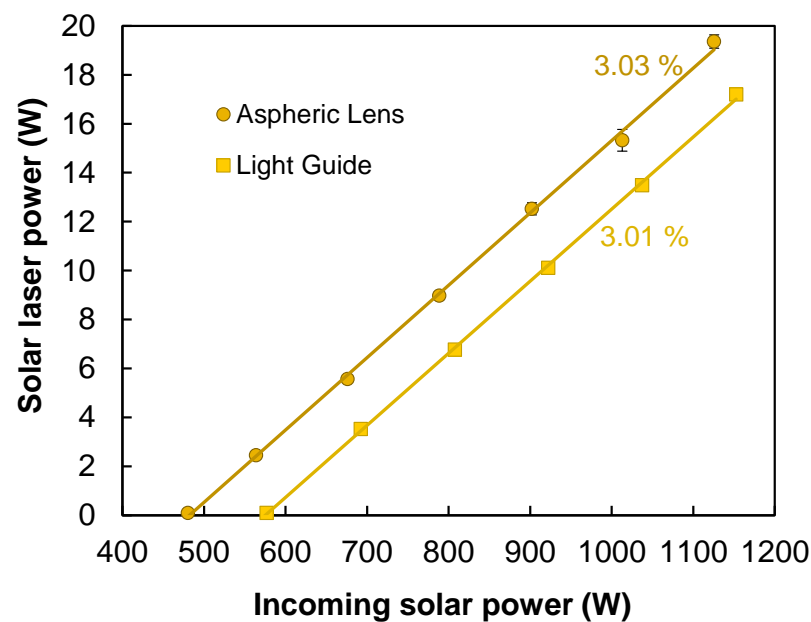
The main difference between these two secondary concentrators relies on the pump light distribution on the laser rod, as shown in Table 1. The absorbed pump light profile within the rod produced by the aspherical lens is more concentrated on its central region because this concentrator preserves the near-Gaussian profile of the pump source. The rectangular light guide enables a uniform absorbed pump light profile within the laser rod as it converts the near-Gaussian profile of the concentrated light source into a uniform rectangular light distribution on the output end. The uniformity of the light absorption on the rod helps to minimize the issues associated to the thermal load.

The Ce:Nd:YAG output performance from two solar laser heads was investigated in PROMES-CNRS, using the MSSF, during February 2022. For both, a short symmetric optical resonator with flat mirrors was used to extract the maximum laser power by the laser rod.

In Table 1 is summarized the output performance of both types of Ce:Nd:YAG side-pumped solar laser heads, and in Figure 6 is shown the laser power as a function of the incoming solar power. The solar laser with the aspherical lens produced 19.6 W laser power at 1064 nm with 1125 W of incoming solar power, corresponding to 18.0 W/m^2 collection efficiency. The solar laser with the light guide produced less laser power, 17.4 W; with slightly more incoming solar power, 1153 W; less solar-to-laser power conversion efficiency; and a higher threshold pump power than the one with the aspherical lens.

Table 1. Summary of the performance of the Ce:Nd:YAG side-pumped solar lasers with the aspherical lens and the rectangular light guide secondary concentrators.

	Aspherical Lens Secondary Concentrator	Light Guide Secondary Concentrator	Improvement of the Aspherical Lens over the Light Guide Concentrator (Times)
Scheme			
Absorbed pump profile			
Laser power (@1064 nm)	19.6 W	17.4 W	1.13
Threshold pump power	480 W	577 W	1.20
Collection efficiency	18.0 W/m^2	16.0 W/m^2	1.13
Slope efficiency	3.0%	3.0%	1.00
Solar-to-laser power conversion efficiency	1.7%	1.5%	1.15
M^2 factor (100% pump power)	30	38	—
M^2 factor (60% pump power)	20	35	—

Figure 6. Solar laser power as a function of the incoming solar power of the Ce:Nd:YAG side-pumped solar lasers with the aspherical lens and the light guide secondary concentrators. Error bars, when not hidden by symbols, are for standard deviation.

The laser beam quality M^2 factors were calculated using Equations (1) and (2). $M_X^2 \approx M_Y^2$ factors of 38 and 35 were determined for the laser beam produced by the solar laser head with the light guide for 100% pump power and 60% of the total pump power, respectively. The M^2 factors measurement of the laser head with the aspherical lens was not possible, because the Ce:Nd:YAG rod fractured before laser beam quality measurements. Thus, they were calculated through numerical analysis by ZEMAX and LASCAD [20], resulting in $M_X^2 \approx M_Y^2$ factors of 30 and 20 for 100% pump power and 60% of the total pump power, respectively. The higher M^2 factors from the laser head with the light guide, compared

with that with the aspherical lens was mainly due to the shorter resonator cavity length of 60 mm, in contrast to the 120 mm of cavity length used with the aspherical lens. The cavity lengths could not be equal in the two cases because of mechanical constraints in the laser head with the aspherical lens. Moreover, the beam quality M^2 factors deteriorated at higher pump power levels, as indicated in Table 1.

The greater laser efficiency produced by the solar laser head with the aspherical lens secondary concentrator can be mainly due to the higher concentration of the incident light in the central region of the laser rod provided by the aspherical lens. However, in an attempt to produce more laser power, by adding more input power, the Ce:Nd:YAG rod fractured on its central zone in the exact region where the solar light was mainly concentrated, as shown in Figure 7a. This event also occurred in a previous study where the Ce:Nd:YAG laser rod was used in an end-side-pumping configuration, in which the solar light was mostly focused on the top region of the rod [25]. This inhomogeneous pumping increased the thermal load of the rod in the region of more pumping intensity, which caused its final fracture when using higher solar powers, limiting the maximum laser output power.
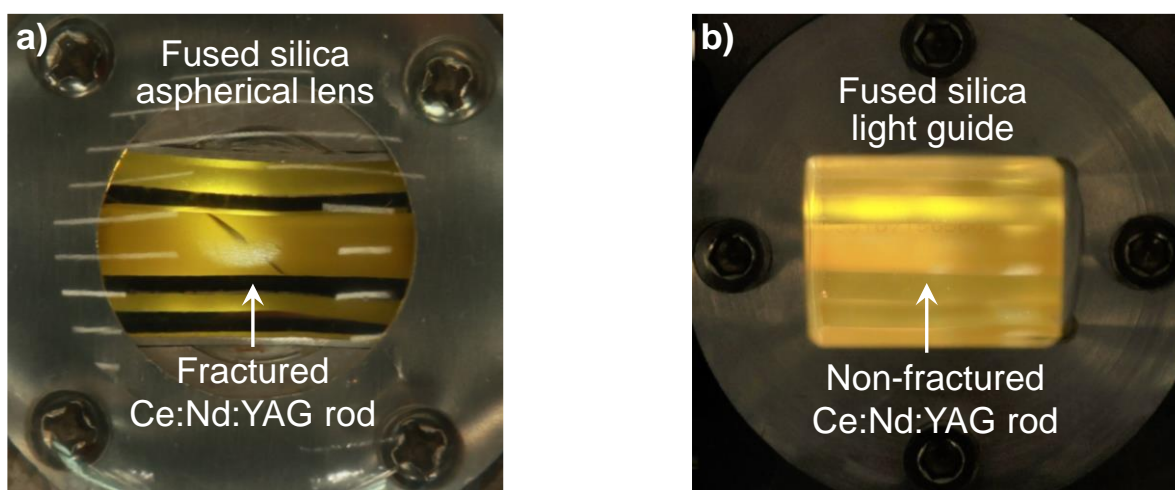
Figure 7. Photograph of the Ce:Nd:YAG laser rods on the laser heads with the fused liquid fused liquid aspheric lens (**a**) and rectangular light guide (**b**) after the solar laser experiments. The fracture on the Ce:Nd:YAG laser rod using the aspheric lens is visible on its central region.

The side-pumping configuration helps to minimize the thermal stress issues in the Ce:Nd:YAG active medium because it spreads the concentrated solar energy along the laser rod axis, which allows a greater increase in the output performance as already demonstrated [26]. Using an aspherical lens as a secondary concentrator enabled the increase in the output laser power; however, since the concentrated solar radiation was not evenly distributed along the laser rod, the absorbed pump distribution was still not uniform (Table 1), which led to Ce:Nd:YAG medium fracture (Figure 7a). The rectangular light guide was able to overcome this problem through the uniformity of the incident solar light on the rod. Although the laser output power was slightly inferior to that of the aspherical lens, the capacity to uniformly distribute the light led to a uniform absorbed pump distribution along the rod (Table 1). The thermal load on the rod was thus considerably reduced, which prevented the Ce:Nd:YAG medium fracture at higher input solar power levels (Figure 7b). Moreover, it also allowed a more stable laser emission during the two-week testing period in PROMES-CNRS without damaging the rod. Therefore, the fused silica light guide with rectangular cross-section is a promising secondary concentrator to enable the laser power scalability of the Ce:Nd:YAG solar laser.

The previous study, based on a Ce:Nd:YAG side-pumped solar laser with a semi-spherical lens as secondary concentrator, was accomplished by using the NOVA heliostat-parabolic mirror system with 75% reflectivity and 66 cm focal length [26], which is more efficient than the MSSF PROMES-CNRS facility with 59% reflectivity and 85 cm focal length.

Nevertheless, the Ce:Nd:YAG rod side-pumped through the NOVA solar facility produced only 16.5 W maximum continuous-wave power at 600 W incoming solar power [26]. In an attempt to boost the laser power by adding more solar power, the Ce:Nd:YAG rod was fractured. In the present study, by using the PROMES-CNRS facility, the Ce:Nd:YAG rod produced 19.6 W maximum continuous-wave laser power, which is 1.19 times more than that from the NOVA facility [26]. More importantly, the Ce:Nd:YAG rod was only fractured at 1125 W incoming solar power level, which is 1.88 times more than that of the previous side-pumped Ce:Nd:YAG laser rod could withstand at the NOVA solar facility. In conclusion, with the PROMES-CNRS solar facility, the solar laser head with aspherical lens offered a much more thermal resistance and a higher solar laser power compared with that obtained with the NOVA facility [26].

It is important to note that the Ce:Nd:YAG active medium is more susceptible to thermal fracture than the Nd:YAG medium when pumped by sunlight. The main reason relies on the Stokes efficiency, which is lower for the Ce:Nd:YAG rod, 0.43 [27] compared with the 0.62 of the Nd:YAG rod [7]. Such low Stokes efficiency results in loss of pump photon energy normally in the form of heat, increasing the thermal load in the rod. Therefore, it is important to design solar laser systems that take this factor into account. The pumping distribution on the active medium plays an important role in the optimization process of scaling solar-pumped lasers to high power.

5. Conclusions

Two solar laser heads with two different secondary concentrators were investigated to study the influence of their pumping distribution on the Ce:Nd:YAG side-pumped solar laser output performance. The solar laser head with the fused silica aspherical lens produced a non-uniform absorbed pump profile within the rod, which is more concentrated on its central region, while the solar laser head with the rectangular fused silica light guide formed a uniform absorbed pump profile along the rod. The laser collection efficiency, solar-to-laser power conversion efficiency, and threshold pump power with the aspherical lens were 18 W/m^2, 1.7%, and 480 W, respectively, which were better than that with the light guide that had 16 W/m^2, 1.5%, and 577 W, respectively. However, the non-uniformity of the absorbed pump profile created by the aspherical lens increased the thermal load of the rod, creating hot pump spots. This led to the Ce:Nd:YAG rod fracture, limiting the maximum laser output power. At the expense of slightly lower solar laser power and efficiency, the use of light guide overcame this problem through the uniformity of the incident solar light on the rod. Therefore, the pumping distribution plays an important role in the design of Ce:Nd:YAG solar laser systems, and the light guide technology may ensure successful solar laser power scaling.

References

1. Lando, M.; Kagan, J.A.; Shimony, Y.; Kalisky, Y.Y.; Noter, Y.; Yogev, A.; Rotman, S.R.; Rosenwaks, S. *Solar-Pumped Solid State Laser Program*; SPIE: Bellingham, WA, USA, 1997; Volume 3110.
2. Vasile, M.; Maddock, C.A. Design of a formation of solar pumped lasers for asteroid deflection. *Adv. Space Res.* **2012**, *50*, 891–905. [CrossRef]
3. Yamada, N.; Ito, T.; Ito, H.; Motohiro, T.; Takeda, Y. Crystalline silicon photovoltaic cells used for power transmission from solar-pumped lasers: III. Prototype for proof of the light trapping concept. *Jpn. J. Appl. Phys.* **2018**, *57*, 08RF07. [CrossRef]
4. Kiss, Z.J.; Lewis, H.R.; Duncan, R.C. Sun pumped continuous optical maser. *Appl. Phys. Lett.* **1963**, *2*, 93–94. [CrossRef]
5. Young, C.G. A Sun-Pumped cw One-Watt Laser. *Appl. Opt.* **1966**, *5*, 993–997. [CrossRef] [PubMed]
6. Arashi, H.; Oka, Y.; Sasahara, N.; Kaimai, A.; Ishigame, M. A Solar-Pumped cw 18 W Nd:YAG Laser. *Jpn. J. Appl. Phys.* **1984**, *23*, 1051–1053. [CrossRef]
7. Weksler, M.; Shwartz, J. Solar-pumped solid-state lasers. *IEEE J. Quantum Electron.* **1988**, *24*, 1222–1228. [CrossRef]
8. Lando, M.; Kagan, J.; Linyekin, B.; Dobrusin, V. A solar-pumped Nd:YAG laser in the high collection efficiency regime. *Opt. Commun.* **2003**, *222*, 371–381. [CrossRef]
9. Dinh, T.H.; Ohkubo, T.; Yabe, T.; Kuboyama, H. 120 watt continuous wave solar-pumped laser with a liquid light-guide lens and an Nd:YAG rod. *Opt. Lett.* **2012**, *37*, 2670–2672. [CrossRef]
10. Liang, D.; Vistas, C.R.; Tiburcio, B.D.; Almeida, J. Solar-pumped Cr:Nd:YAG ceramic laser with 6.7% slope efficiency. *Sol. Energy Mater. Sol. Cells* **2018**, *185*, 75–79. [CrossRef]
11. Ohkubo, T.; Yabe, T.; Yoshida, K.; Uchida, S.; Funatsu, T.; Bagheri, B.; Oishi, T.; Daito, K.; Ishioka, M.; Nakayama, Y.; et al. Solar-pumped 80 W laser irradiated by a Fresnel lens. *Opt. Lett.* **2009**, *34*, 175–177. [CrossRef]
12. Almeida, J.; Liang, D.; Vistas, C.R.; Guillot, E. Highly efficient end-side-pumped Nd:YAG solar laser by a heliostat-parabolic mirror system. *Appl. Opt.* **2015**, *54*, 1970–1977. [CrossRef] [PubMed]
13. Liang, D.; Almeida, J.; Vistas, C.R. 25 W/m^2 collection efficiency solar-pumped Nd:YAG laser by a heliostat-parabolic mirror system. *Appl. Opt.* **2016**, *55*, 7712–7717. [CrossRef] [PubMed]
14. Liang, D.; Almeida, J.; Vistas, C.R.; Guillot, E. Solar-pumped Nd:YAG laser with 31.5 W/m^2 multimode and 7.9 W/m^2 TEM00-mode collection efficiencies. *Sol. Energy Mater. Sol. Cells* **2017**, *159*, 435–439. [CrossRef]
15. Guan, Z.; Zhao, C.; Zhang, H.; Li, J.; He, D.; Almeida, J.; Vistas, C.R.; Liang, D. 5.04% system slope efficiency solar-pumped Nd:YAG laser by a heliostat-parabolic mirror system. *J. Photonics Energy* **2018**, *8*, 027501. [CrossRef]
16. Guan, Z.; Zhao, C.; Li, J.; He, D.; Zhang, H. 32.1 W/m^2 continuous wave solar-pumped laser with a bonding Nd:YAG/YAG rod and a Fresnel lens. *Opt. Laser Technol.* **2018**, *107*, 158–161. [CrossRef]
17. Vistas, C.R.; Liang, D.; Almeida, J.; Tibúrcio, B.D.; Garcia, D. A doughnut-shaped Nd:YAG solar laser beam with 4.5 W/m^2 collection efficiency. *Sol. Energy* **2019**, *182*, 42–47. [CrossRef]
18. Liang, D.; Almeida, J. Solar-Pumped TEM$_{00}$ Mode Nd:YAG laser. *Opt. Express* **2013**, *21*, 25107–25112. [CrossRef]
19. Liang, D.; Almeida, J.; Vistas, C.R.; Guillot, E. Solar-pumped TEM$_{00}$ mode Nd:YAG laser by a heliostat-Parabolic mirror system. *Sol. Energy Mater. Sol. Cells* **2015**, *134*, 305–308. [CrossRef]
20. Vistas, C.R.; Liang, D.; Almeida, J.; Guillot, E. TEM$_{00}$ mode Nd:YAG solar laser by side-pumping a grooved rod. *Opt. Commun.* **2016**, *366*, 50–56. [CrossRef]
21. Bouadjemine, R.; Liang, D.; Almeida, J.; Mehellou, S.; Vistas, C.R.; Kellou, A.; Guillot, E. Stable TEM$_{00}$-mode Nd:YAG solar laser operation by a twisted fused silica light-guide. *Opt. Laser Technol.* **2017**, *97*, 1–11. [CrossRef]
22. Mehellou, S.; Liang, D.; Almeida, J.; Bouadjemine, R.; Vistas, C.R.; Guillot, E.; Rehouma, F. Stable solar-pumped TEM$_{00}$-mode 1064 nm laser emission by a monolithic fused silica twisted light guide. *Sol. Energy* **2017**, *155*, 1059–1071. [CrossRef]
23. Liang, D.; Vistas, C.R.; Almeida, J.; Tiburcio, B.D.; Garcia, D. Side-pumped continuous-wave Nd:YAG solar laser with 5.4% slope efficiency. *Sol. Energy Mater. Sol. Cells* **2019**, *192*, 147–153. [CrossRef]
24. Yagi, H.; Yanagitani, T.; Yoshida, H.; Nakatsuka, M.; Ueda, K. The optical properties and laser characteristics of Cr^{3+} and Nd^{3+} co-doped Y3Al5O12 ceramics. *Opt. Laser Technol.* **2007**, *39*, 1295–1300. [CrossRef]
25. Vistas, C.R.; Liang, D.; Garcia, D.; Almeida, J.; Tibúrcio, B.D.; Guillot, E. Ce:Nd:YAG continuous-wave solar-pumped laser. *Optik* **2020**, *207*, 163795. [CrossRef]
26. Vistas, C.R.; Dawei, L.; Joana, A.; Bruno, D.T.; Dário, G.; Miguel, C.; Hugo, C.; Emmanuel, G. Ce:Nd:YAG side-pumped solar laser. *J. Photonics Energy* **2021**, *11*, 018001. [CrossRef]
27. Villars, B.; Steven Hill, E.; Durfee, C.G. Design and development of a high-power LED-pumped Ce:Nd:YAG laser. *Opt. Lett.* **2015**, *40*, 3049–3052. [CrossRef]

28. Meng, J.X.; Li, J.Q.; Shi, Z.P.; Cheah, K.W. Efficient energy transfer for Ce to Nd in Nd/Ce codoped yttrium aluminum garnet. *Appl. Phys. Lett.* **2008**, *93*, 221908. [CrossRef]

29. Samuel, P.; Yanagitani, T.; Yagi, H.; Nakao, H.; Ueda, K.I.; Babu, S.M. Efficient energy transfer between Ce^{3+} and Nd^{3+} in cerium codoped Nd: YAG laser quality transparent ceramics. *J. Alloys Compd.* **2010**, *507*, 475–478. [CrossRef]

30. Li, Y.; Zhou, S.; Lin, H.; Hou, X.; Li, W. Intense 1064nm emission by the efficient energy transfer from Ce^{3+} to Nd^{3+} in Ce/Nd co-doped YAG transparent ceramics. *Opt. Mater.* **2010**, *32*, 1223–1226. [CrossRef]

31. Guo, Y.; Huang, J.; Ke, G.; Ma, Y.; Quan, J.; Yi, G. Growth and optical properties of the Nd, Ce:YAG laser crystal. *J. Lumin.* **2021**, *236*, 118134. [CrossRef]

32. Payziyev, S.; Sherniyozov, A.; Bakhramov, S.; Zikrillayev, K.; Khalikov, G.; Makhmudov, K.; Ismailov, M.; Payziyeva, D. Luminescence sensitization properties of Ce: Nd: YAG materials for solar pumped lasers. *Opt. Commun.* **2021**, *499*, 127283. [CrossRef]

33. *ASTM G173-03*; Standard tables for reference solar spectral irradiances: Direct normal and hemispherical on 37° tilted surface. ASTM International: West Conshohocken, PA, USA, 2012.

34. Nishiura, S.; Tanabe, S.; Fujioka, K.; Fujimoto, Y. Properties of transparent Ce:YAG ceramic phosphors for white LED. *Opt. Mater.* **2011**, *33*, 688–691. [CrossRef]

35. Prahl, S. Nd:YAG—Nd:Y3Al5O12. Available online: https://omlc.org/spectra/lasermedia/html/052.html (accessed on 5 April 2022).

36. Tai, Y.; Zheng, G.; Wang, H.; Bai, J. Near-infrared quantum cutting of Ce^{3+}–Nd^{3+} co-doped $Y_3Al_5O_{12}$ crystal for crystalline silicon solar cells. *J. Photochem. Photobiol. A* **2015**, *303*, 80–85. [CrossRef]

37. Mares, J.; Jacquier, B.; Pédrini, C.; Boulon, G. Energy transfer mechanisms between Ce^{3+} and Nd^{3+} in YAG: Nd, Ce at low temperature. *Rev. Phys. Appl.* **1987**, *22*, 145–152. [CrossRef]

38. Yamaga, M.; Oda, Y.; Uno, H.; Hasegawa, K.; Ito, H.; Mizuno, S. Energy transfer from Ce to Nd in $Y_3Al_5O_{12}$ ceramics. *Phys. Status Solidi C* **2012**, *9*, 2300–2303. [CrossRef]

39. Wegh René, T.; Donker, H.; Oskam Koenraad, D.; Meijerink, A. Visible Quantum Cutting in $LiGdF_4$:Eu^{3+} Through Downconversion. *Science* **1999**, *283*, 663–666. [CrossRef]

40. Liu, X.; Teng, Y.; Zhuang, Y.; Xie, J.; Qiao, Y.; Dong, G.; Chen, D.; Qiu, J. Broadband conversion of visible light to near-infrared emission by Ce^{3+}, Yb^{3+}-codoped yttrium aluminum garnet. *Opt. Lett.* **2009**, *34*, 3565–3567. [CrossRef]